

Extended SO₂ outgassing from the 2014–2015 Holuhraun lava flow field, Iceland

Isla C. Simmons¹ · Melissa A. Pfeffer² · Eliza S. Calder¹ · Bo Galle³ · Santiago Arellano³ · Diego Coppola⁴ · Sara Barsotti²

Received: 18 January 2017 / Accepted: 27 September 2017 / Published online: 27 October 2017
© The Author(s) 2017. This article is an open access publication

Abstract The 2014–2015 Holuhraun eruption was the largest fissure eruption in Iceland in the last 200 years. This flood basalt eruption produced ~ 1.6 km³ of lava, forming a lava flow field covering an area of ~ 84 km². Over the 6-month course of the eruption, ~ 11 Mt of SO₂ were released from the eruptive vents as well as from the cooling lava flow field. This work examines the post-eruption SO₂ flux emitted by the Holuhraun lava flow field, providing the first study of the extent and relative importance of the outgassing of a lava flow field after emplacement. We use data from a scanning differential optical absorption spectroscopy (DOAS) instrument installed at the eruption site to monitor the flux of SO₂. In this study, we propose a new method to estimate the SO₂ emissions from the lava flow field, based on the characteristic shape of the scanned column density distribution of a homogenous source close to the ground. Post-eruption outgassing of the lava flow field continued for at least 3 months after the end of the eruption, with SO₂ flux between < 1 and 9 kg/s. The lava flow field post-eruption emissions were not a significant contributor to the total SO₂ released during the eruption; however, the lava flow field was still an important polluter and caused high concentrations of SO₂ at ground level after lava effusion ceased.

Keywords SO₂ · Lava · DOAS · Post-eruption outgassing

Introduction

A dyke-fed basaltic fissure eruption from the Bárðarbunga volcanic system occurred from 31 August 2014 until 27 February 2015 (Icelandic Meteorological Office (IMO), 2015a). The fissure was located to the north of the Vatnajökull icecap, forming the 2014–2015 Holuhraun lava flow field (Fig. 1). The eruption produced 1.6 ± 0.3 km³ of lava, forming an 84.1 ± 0.6 km² lava flow field (Gislason et al. 2015). This classifies the eruption as a flood basalt eruption following Thordarson and Larsen (2007). This makes the Holuhraun eruption the most voluminous effusive eruption in Iceland since the 1783–1784 Laki eruption (Schmidt et al. 2015).

This work provides a new approach for measuring SO₂ emissions from a lava flow field after emplacement. Several studies have investigated the impacts of the Holuhraun eruption on populations and the environment (e.g. Gislason et al. 2015; Ilyinskaya et al. 2017). Establishing the potential duration and magnitude of post-eruptive SO₂ outgassing will increase resilience in vulnerable communities related to the health hazards caused by SO₂ after future eruptions. We additionally discuss the physical processes of cooling and fracturing (e.g. Keszthelyi and Denlinger, 1996; Kattenhorn and Schaefer, 2008; Patrick et al. 2004; Wittmann et al. 2017) that contribute to post-emplacement lava outgassing.

Volatile outgassing during and after eruption

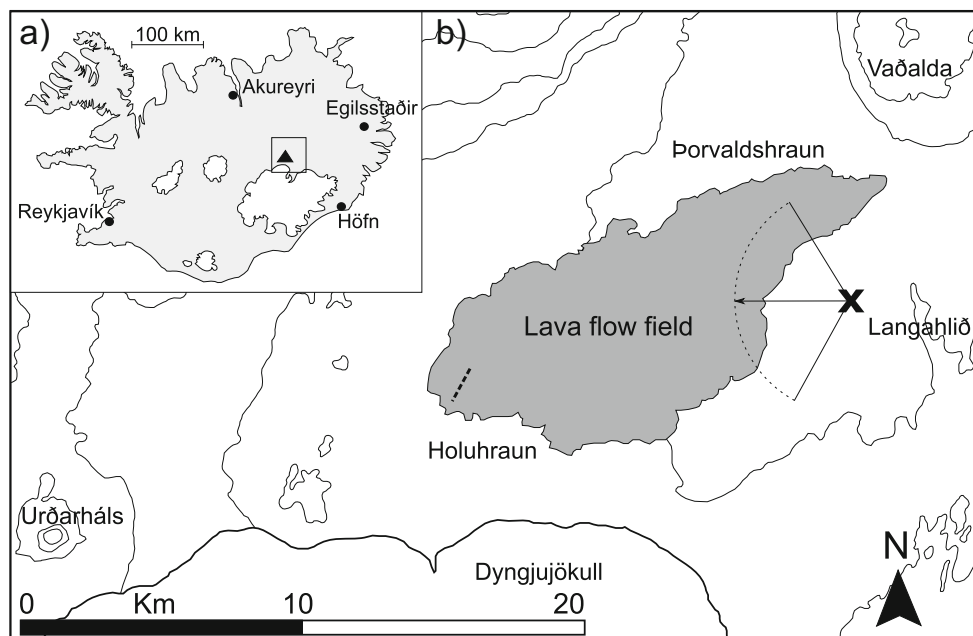
Gases dissolved within magma are transferred to the atmosphere by degassing. The term “degassing” is used to describe the process by which a magma loses its volatiles (Burgisser

Editorial responsibility: T.P. Fischer

✉ Isla C. Simmons
isla.simmons@ed.ac.uk

- ¹ School of GeoSciences, The University of Edinburgh, Edinburgh, UK
- ² Icelandic Meteorological Office, Reykjavík, Iceland
- ³ Department of Space, Earth and Environment, Chalmers University of Technology, Gothenburg, Sweden
- ⁴ Department of Earth Science, University of Torino, Torino, Italy

Fig. 1 **a** Map of Iceland showing the location of the eruption (triangle). **b** The location of the 2014–2015 Holuhraun eruption site. The fissure is represented by the dashed line and the area of the lava flow field is highlighted. The location of ScanDOAS instrument MAYP111126 is indicated by the symbol “x”. The viewing direction (arrow) and scanning sector (arc segment) of the instrument are shown. Base maps from the Icelandic Meteorological Office (IMO), 2015b



and Degruyter, 2015). This includes exsolution of gas from the melt, gas segregation, and outgassing (e.g. Bottinga and Javoy, 1991; Sparks, 2003; Palma et al. 2008). Following Burgisser and Degruyter (2015) and Palma et al. (2008, 2011), we define “outgassing” only as the release of this gas to the atmosphere.

Basaltic fissure eruptions release large volumes of SO_2 into the atmosphere. Basaltic magmas have a high sulphur yield, which is typically two to four times higher than silicic magmas (Thordarson et al. 2003). As a result, SO_2 is released during basaltic flood eruptions by a two-stage degassing process: from the magma as it rises through the conduit and erupts at the vent and from lava flows during and after their emplacement (Walker, 1989; Thordarson et al. 1996; Thordarson et al. 2003). Gases released at the vent, and associated with degassing of volatiles as the magma approaches the surface, contribute to an eruption plume. Gases released from lava flows will remain close to ground level forming a low-level haze (Fig. 2).

Swanson and Fabbi (1973) studied volatile loss during isothermal flow of pāhoehoe lava in lava tubes at Mauna Ulu, Kilauea (Hawaii). They observed that the majority of sulphur was released soon after eruption (60% was lost during flow over a distance of 12 km), but lava flows were observed to continue outgassing for at least 2 to 4 h after solidification (Swanson and Fabbi, 1973). In contrast, the Holuhraun lava flow field exhibits a wide range of lava morphologies, varying from pāhoehoe to ‘a’ā (Pedersen et al. 2017) and, as demonstrated by this work, continued to release sulphur volatiles for several months after emplacement.

In another study on Hawaiian flows, Bottinga and Javoy (1991) proposed that lava flows degas volatiles during

transportation because their temperature decreases. The resulting supersaturation of volatiles within the lava increases, causing exsolution resulting in bubble formation. Cashman et al. (1994) proposed that volatiles were primarily released from active lava flows by the rise and escape of bubbles already contained within the lava. Sparks and Pinkerton (1978) noted that as lava is degassed, exsolution of gas results in undercooling of the lava. This leads to crystallisation and causes an increase in viscosity and yield strength (Sparks and Pinkerton, 1978). Mechanical processes during the flow of lava then cause the solidified crust to fracture (e.g. Polacci and Papale, 1997; Soule and Cashman, 2004), allowing further gas to be released.

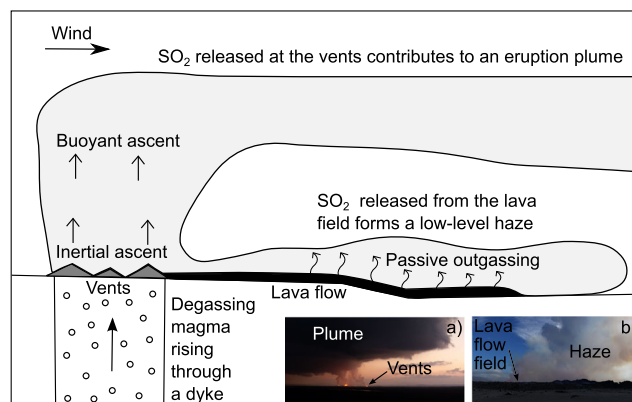


Fig. 2 Two-stage degassing during basaltic fissure eruptions: SO_2 is released at vents contributing to an eruption plume and from lava flows forming a low-level haze. Adapted from Thordarson and Self (2003). Inset images show **a** the Holuhraun eruption plume and **b** gas released by the lava flow field. Photos by B. Bergsson (IMO)

Many studies have investigated the degassing of lava flows as they are actively flowing from the vent; however, little discussion exists about the processes of extended outgassing following lava flow emplacement. The studies of Bottinga and Javoy (1991) and Cashman et al. (1994) both examine the release of gases from flowing lava and are therefore insufficient to explain the continued flux of SO₂ from the Holuhraun lava flow field for several months after its emplacement and solidification. We thus, here, consider the physical processes which occur over the longer time period that was captured by our outgassing measurements.

Volcanic SO₂ monitoring

SO₂ emission measurements have been fundamental to volcanic monitoring since the development of the correlation spectrometer (COSPEC) in the 1970s (Moffat and Millan, 1971; Stoiber et al. 1983). Malinconico (1979) observed that increases in SO₂ flux at Mt. Etna, Italy, corresponded to increases in volcanic activity, suggesting that SO₂ fluctuations can be used to predict eruptions. SO₂ flux has since been observed to correlate with volcanic activity (Soufrière Hills, Montserrat; Edmonds et al. 2003), magma extrusion rate (Unzen, Japan; Hirabayashi et al. 1995), seismicity during explosive activity (Merapi, Indonesia; Jousset et al., 2013), and lava lake activity (Villarrica, Chile; Palma et al. 2008, and Erebus, Antarctica; Kyle et al. 1994).

Differential optical absorption spectroscopy (DOAS) was also developed in the 1970s, as a method for measuring atmospheric gases (Platt et al. 1979). It has since been used to measure SO₂ emissions of volcanoes worldwide (e.g. Edner et al. 1994; Weibring et al. 1998; McGonigle et al. 2002) and has now superseded COSPEC as the primary volcanic SO₂ flux monitoring technique (Galle et al. 2002; Bobrowski et al. 2010). Measurement of volcanic plumes was further enhanced by the development of the SO₂ camera (Mori and Burton, 2006; Bluth et al. 2007), providing high temporal resolution SO₂ flux measurements and allowing SO₂ heterogeneity within the plume to be quantified (Bluth et al. 2007). SO₂ measurement techniques have been employed to determine SO₂ emissions within volcanic plumes, both during eruptive episodes (e.g. Jousset et al. 2013; Gíslason et al. 2015) and during passive degassing (e.g. McGonigle et al. 2002; Sawyer et al. 2008); however, this work provides the first attempt at using DOAS to measure the SO₂ released by an emplaced lava flow field.

The 2014–2015 Holuhraun eruption

Over the 6-month course of the Holuhraun eruption, 11 ± 5 Mt of SO₂ were emitted (Gíslason et al. 2015), with average emission rates of 400 kg/s and peaks of over 1000 kg/s (Barsotti et al. 2015; Gauthier et al. 2016). The majority of

gases were released from the eruption fissure and contributed to an eruption plume that contained very little ash but was concentrated in SO₂ and H₂O (Gíslason et al. 2015). In addition to the principal eruption plume, SO₂ was also released directly from the lava flows, forming a low-level haze of SO₂. A surveillance flight on 4 November 2014, for example, revealed a distinct two-layered gas cloud that included a low-level “haze” of H₂O (both magmatic and meteoric), SO₂, and other volcanic gases. This haze rose from the lava flow field to an elevation of 700 m above ground level, with the eruption plume ascending to an elevation of 1500–2500 m (Fig. 3; IMO, 2014). High concentrations of SO₂ were measured at ground level throughout Iceland, and in many communities, the health standard of 350 µg/m³/h was exceeded, posing health risks to the population (Gíslason et al. 2015, Ilyinskaya et al. 2017). After the eruption ceased at the end of February 2015, high concentrations of SO₂ continued to be detected at ground level near to the eruption site but dropped to background levels at communities downwind (IMO, 2015a; Umhverfisstofnun, 2016). The aim of this work was to measure the SO₂ released from the cooling lava flow field after the eruption and to examine the processes that facilitate an emplaced, cooling lava flow field to outgas over a prolonged period.

Methods

The methodology used to derive the SO₂ flux from the lava flow field was based on the same principle as is used in COSPEC and MobileDOAS measurements of an elevated gas plume (e.g. Stoiber et al. 1983; Galle et al. 2002). Following this approach, the vertical column density (VCD) of a gas is measured using absorption spectroscopy with the

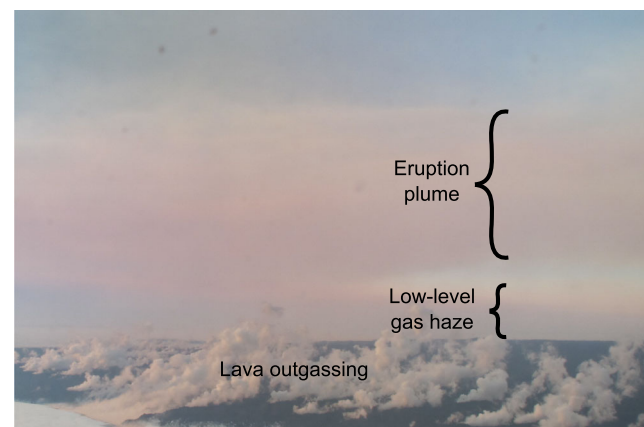


Fig. 3 A photo taken during the surveillance flight on 4 November 2014 showing the low-level gas haze and the higher-level eruption plume. Gases (including H₂O, both magmatic and meteoric, SO₂, and CO₂) can be seen rising from fractures in the lava flow field. Photo by M. Hensch, IMO

sky as the light source (Platt and Stutz, 2008). By traversing under the plume in a direction approximately perpendicular to the plume propagation, and integrating the obtained vertical column amounts, the total number of molecules in a cross section of the plume may be determined. After multiplication with the plume speed, the total gas emission is calculated (e.g. Edner et al. 1994; Galle et al., 2002; McGonigle et al. 2002; Edmonds et al. 2003; Platt et al. 2015).

In our application, a stationary scanning DOAS instrument (ScanDOAS; Galle et al. 2010) was used to determine the VCD of the low-level haze of gas emitted by the lava flow field. To make this measurement, we assume that the lava flow field produces a gas layer close to the ground with uniform thickness. We also assume that this layer has a width that is equal to the maximum width of the lava flow field, measured in a direction perpendicular to the wind direction, the “effective haze width”. Using this geometry, with a ScanDOAS instrument, we can determine the VCD at the instrument location, and using the known wind direction and shape of the lava flow field, we can derive the effective haze width. The gas flux can then be determined by multiplying the VCD at the instrument site with the effective haze width and with the wind speed.

Measurement geometries

A ScanDOAS scans the sky from horizon to horizon in a vertical plane approximately perpendicular to the plume propagation, recording radiance spectra of the diffused UV solar radiation received at each angle (Edmonds et al. 2003). The “slant column density” (SCD) of SO₂ from each spectrum is calculated by differential optical absorption spectroscopy (DOAS), and the integral of column densities at all angles is then multiplied by the plume speed to obtain the flux of SO₂ (e.g. Stoiber et al. 1983; Galle et al. 2002; McGonigle et al. 2002). The instrument typically makes one scan approximately every 5 min, each scan being composed of 26 spectra.

In a variation on this “flat” scan geometry, the scan is made over a conical surface with its tip at the instrument and its base through the gas source. The main advantage of this “conical” geometry is that a wider range of plume directions may be covered by a single instrument (Galle et al. 2010). In this study, a conical geometry with an opening angle of 60° was used. The instrument used in our study is a modification of the standard NOVAC-Mark I instrument (NOVAC: Network for Observation of Volcanic and Atmospheric Change; Galle et al. 2010), with a non-rotating, cylindrical external hood made of quartz, and a UV-sensitive OceanOptics MAYA Pro spectrometer (<http://oceanoptics.com/wp-content/uploads/OEM-Data-Sheet-Maya2000Prov3.pdf>).

SO₂ emissions from a vent will contribute to an elevated eruption plume, which will be identified on a DOAS scan as a concentrated distribution of SO₂ column densities, with higher

columns observed at elevation angles in which the scanner detects the bulk of the plume (Fig. 4a). In contrast, SO₂ emissions from a lava flow field or a grounded plume will form a dispersed low-level haze. This will have a characteristic trough shape on a DOAS scan (Fig. 4b). When scanning through a low-level haze of SO₂, the optical path will be greater at low elevation angles close to the ground, producing a greater SO₂ slant column density. The minimum slant column densities of SO₂ will be observed at the highest elevation angles, where the shortest path through the haze is sampled (Fig. 4b). With flat geometry, this occurs at the zenith, but for the conical geometry used here, this condition is met at 30° from the zenith.

Determination of the SO₂ vertical column density at the measurement site

If we assume a layer of gas close to the ground, and flat scan geometry, then the slant column densities (SCD) can be expressed as:

$$\text{SCD} = \text{VCD}/\cos(\alpha) \quad (1)$$

where VCD is the vertical column density through the sampled layer and α is the scan angle measured from the zenith.

In a standard evaluation of a DOAS spectrum, the spectrum measured through the gas plume is divided by a clean air reference spectrum, typically obtained in a direction with no gas (Galle et al. 2002; Edmonds et al. 2003). In this way, spectral features related to the sky spectra as well as instrumental features are cancelled out and an absorption spectrum of the gas plume is obtained. When scanning through a low-level haze, all spectra, including the reference spectrum, will contain SO₂. Our goal was therefore to determine the VCD without having access to a clean air reference spectrum. In this case, the derived slant column was the difference between the slant column of the measured spectrum and the slant column of the reference spectrum by which it was divided. For a flat geometry, this can be achieved by dividing a spectrum taken at $\alpha = 60^\circ$ with a reference spectrum taken at $\alpha = 0^\circ$. The resulting SCD_{diff} is equal to VCD/0.5 - VCD/1, which is in turn equal to VCD, and thus provides the required VCD.

For a conical geometry, the same method can be applied. However, here the relation between VCD and SCD becomes:

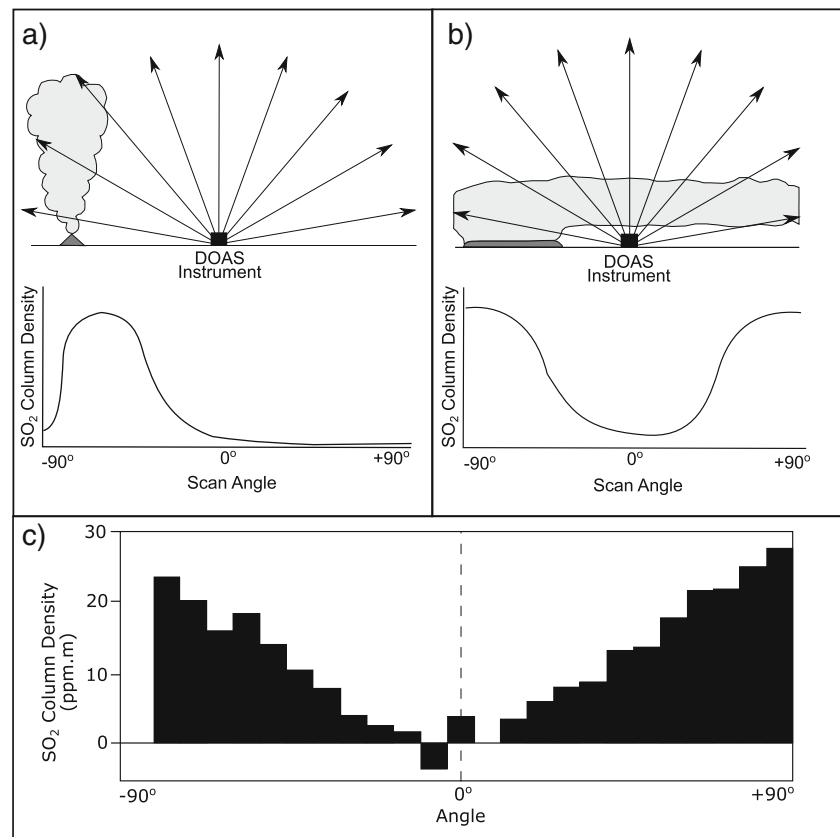
$$\text{SCD} = \text{VCD}/[\cos(\alpha) \times \sin(\beta)] \quad (2)$$

With the conical angle $\beta = 60^\circ$, the difference between the SCD taken at angles $\alpha = 60^\circ$ and $\alpha = 0^\circ$ becomes:

$$\text{SCD}_{\text{diff}} = \text{VCD}/0.866 \quad (3)$$

Therefore, to obtain the VCD at the instrument location, we multiply the average SCD obtained at angles $\alpha = 60^\circ$ and

Fig. 4 Schematic illustration of the characteristic shapes recorded by scanning DOAS when scanning vertically through **a** an eruption plume produced by SO_2 released at a vent and **b** a low-level haze produced by SO_2 released from a lava flow. **c** DOAS scan from 11:57 UTC on 7 March 2015 showing the characteristic trough shape of a scan made through the low-level SO_2 haze released by the Holuhraun lava flow field. Black columns are the SO_2 column densities at incremental angles



$\alpha = 0^\circ$ by 0.866. The SCD and VCD are, by convention, expressed in ppm*m (parts per million-metre). To calculate SO_2 emission, these are converted to kg/m^2 by applying the ideal gas law and multiplying the VCD (in ppm*m) by 2.66×10^{-6} .

Field configuration and SO_2 flux calculation

ScanDOAS instruments were installed at the Holuhraun eruption site by the Icelandic Meteorological Office and Chalmers University (Gothenburg, Sweden) to measure SO_2 emissions during the eruption. Instrument MAYP111126 (cross symbol in Fig. 1) was installed at its location to the east of the lava flow field on 4 March 2015, where it was oriented towards the west and optimally located for viewing of the lava flow field. This occurred after the eruption ended on 27 February, and data from this spectrometer were used to calculate the post-eruptive SO_2 flux from the lava flow field.

All scans from instrument MAYP111126, from its installation on 4 March 2015 until 31 May 2015, were examined to identify those with the characteristic trough shape that represented the anticipated view through a low-level haze of SO_2 from the lava flow field (Fig. 4c). Each “haze” scan was first re-evaluated between 310 and 325 nm using the NovacProgram software (version 1.82; Galle et al. 2010), including additional spectra in the DOAS fitting process to

account for the presence of ozone in the atmosphere and the “Ring effect” (i.e. the “filling-in” of deep absorption features, such as the solar Fraunhofer lines, in a measured atmospheric spectrum, which is caused by inelastic (Raman) scattering of light by air molecules (Grainger and Ring, 1962)). After calculating the column densities, a quality check was applied to ensure that scans retained the characteristic trough shape of the anticipated lava flow field “haze” scans. To ensure a symmetrical trough shape, scans were excluded if slant column densities at $+60^\circ$ and -60° differed by more than 20%. To calculate the SO_2 flux (in kg/s) recorded by each scan, the measured VCD of SO_2 (in kg/m^2) was multiplied by the effective width of the SO_2 haze (in m) and the haze speed (in m/s), assumed to be equivalent to the wind speed measured at a co-located meteorological station.

As mentioned above, the effective width of the low-level haze produced by the lava flow field was assumed to be equal to the total width of the lava flow field, measured in a direction perpendicular to the wind direction (Fig. 5). Because the lava flow field has an irregular shape, this width varies with different wind directions and can be measured from a map showing the extension of the lava flow field. The minimum effective haze width occurs when the wind blows along the longer dimension of the lava flow field, and as wind direction deviates from this, the effective haze width increases (Fig. 5).

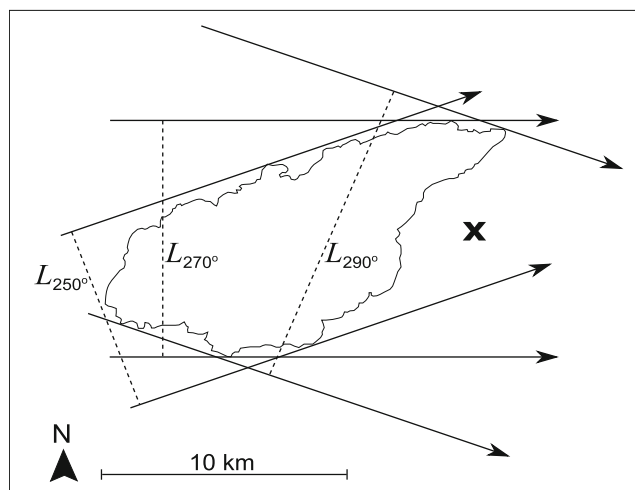


Fig. 5 The effective plume width (L) is the maximum width of the lava flow field in the direction perpendicular to the wind direction. The diagram shows the effective plume widths (dashed lines) for wind directions (arrows) of 250° , 270° (directly towards the viewing direction of the ScanDOAS instrument), and 290° . The location of ScanDOAS instrument MAYP111126 is indicated by the symbol “x”

Wind speed and direction were recorded every 10 min using a meteorological station installed at the eruption site. Scans were filtered by wind direction, with scans included only when the wind was blowing towards the instrument ($\pm 20^\circ$).

Lava flow field radiant heat flux

The radiant heat flux of the Holuhraun lava flow field was estimated using MODIS (Moderate Resolution Imaging Spectroradiometer), provided by the MIROVA (Middle InfraRed Observation of Volcanic Activity) system of Coppola et al. (2016). During the effusive crisis, the MIROVA system allowed automatic measurements of the volcanic radiative power (VRP) sourced from the active lava flow field, and related effusion rates (Coppola et al., 2017). However, the VRP provided automatically by MIROVA is based on the simple heat flux conversion approach of Wooster et al. (2003) that works for active lava flows with high surface temperatures (> 600 K). This approach begins to fail for cooling surfaces, especially below 200°C , which is the case of the post-eruption Holuhraun lava flow field. For this post-eruptive period, we thus recalculate the radiant heat flux as:

$$Q_{\text{rad}} = \sigma \varepsilon A_{\text{flow}} \left(BT_{\text{MIR, flow}}^4 - BT_{\text{MIR, bk}}^4 \right) \quad (4)$$

where σ is the Stefan-Boltzmann constant ($5.67051 \times 10^{-8} \text{ W/m}^2/\text{K}^4$), ε is the emissivity of the lava surface (assumed to be 0.95 for basalt; Patrick et al. 2004), A_{flow} is the final area of the cooling lava flow field (84 km^2 ; Pedersen et al. 2017), and $BT_{\text{MIR, flow}}$ and $BT_{\text{MIR, bk}}$ are the average brightness

temperatures of the flow surface pixels and surrounding background, respectively, calculated from selected MODIS-MIROVA cloud-free images (Fig. 6).

Uncertainty and error

Individual SO_2 flux measurements were calculated as the product of the average vertical column density (VCD), effective haze width, and wind speed. Thus, the total uncertainty on the flux measurement can be obtained by determining the uncertainties of these three independently derived quantities. The uncertainty on the average VCD depends on two factors: the intrinsic uncertainty of the retrieved SCDs at various angles and the uncertainty related to the method used to derive the mean VCD from a set of SCDs in one scan. The typical uncertainty of a DOAS SCD has been characterised for NOVAC instruments by Galle et al. (2010) and is expected to be around 15%. The sources of this uncertainty include added UV radiation by scattering between the plume and the instrument (Mori et al. 2006), uncertainty in the reference absorption cross sections used in the retrieval (Stutz and Platt, 1996), and possible distortions of the sensor response function due to temperature or other environmental effects (Galle et al. 2010).

The method proposed to derive a representative VCD is based on the assumption that a homogenous layer of gas surrounds the instrument. For each scan that contains a set of 26 SCDs taken at steps of 7.2° from horizon to horizon, this assumption results in a trough shape of the distribution of these SCDs. This occurs because the shortest column corresponds to the shortest path through the haze layer, when the scanner looks upwards, and then progressively increases with scan angle, as path length through the haze layer increases (see Fig. 4). Thus, the measurements used in this study were selected by visual inspection of each scan, i.e. only scans with the expected trough-shaped distribution of SCDs were used for analysis. In addition, a numerical filter was applied to use only symmetrical scans, where the columns at $+60^\circ$ and -60° differed by less than 20%. A conservative uncertainty related to this method may be 20%, allowing for imperfect scanning geometry, radiative transfer, and natural variability of the columns in the layer. Each VCD thus has a total uncertainty of $\sim 35\%$.

The uncertainty related to the effective haze width depends on the stability of the wind direction and accuracy in the determination of the dimensions of the lava flow field. The wind direction used here was measured by a meteorological station in close proximity to the scanning system, and these data were in good agreement with measurements from another station operated by IMO 20 km further away. This suggests that wind directions close to ground level were relatively stable over a large area, in spite of the presence of a hot lava flow field and a cold glacier. The accuracy of the effective haze width for different wind directions must also be considered. From a

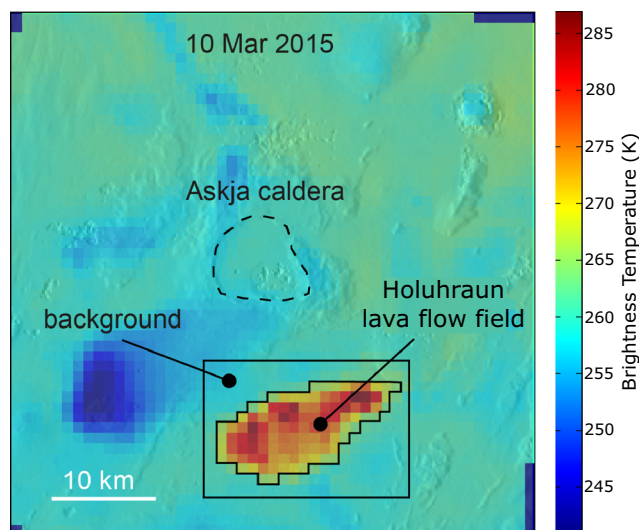


Fig. 6 MIROVA thermal map (1-km resolution) of the lava flow field and surrounding region produced from a MODIS image acquired at 04:00 UTC on 10 March 2015 during the post-eruption cooling phase. The map represents the brightness temperature (in K) recorded by the MIR channel of MODIS (centred at $\sim 3.9 \mu\text{m}$). Note the temperature anomaly due to the presence of the Holuhraun lava flow field to the south of Askja caldera

map of the extent of the lava flow field, the maximum widths of the lava flow field in directions perpendicular to wind directions in the range 250° to 290° were measured (Fig. 5). This range of wind directions corresponds to the possible directions that would produce a haze above the instrument, which was oriented at 270° . Because our study took place after the eruption had ended, the extent of the lava flow field itself can be considered unchanging. Assuming that the measurements of haze widths from a map can be achieved with an accuracy of 1%, and that wind directions vary (spatially and temporarily) within 20%, the total uncertainty on haze width is of the order of 20%.

Finally, uncertainty related to the haze speed must be determined. It is assumed here that haze speed is equal to wind speed close to the ground. We attribute a value of 20% to this uncertainty, following Galle et al. (2002) and Edmonds et al. (2003). Therefore, the total uncertainty of a single flux measurement is estimated to be, quite conservatively, 45%. The total uncertainty is calculated by summing in “quadrature” the uncertainty of all variables, that is, the relative uncertainty of the flux is equal to the square root of the sum of the squares of the relative uncertainties of the variables, i.e. $\sqrt{(0.35^2 + 0.2^2 + 0.2^2)} = 0.45$.

Results

Lava flow field SO_2 flux

Post-eruption SO_2 fluxes from the Holuhraun lava flow field were calculated as varying between < 1 and 9 kg/s (Fig. 7). In

the 3 months following the eruption, the lava flow field released an average of 3 kg/s of SO_2 (standard deviation 1.9 kg/s). We found no overall trend in SO_2 emission with time; instead, the SO_2 outgassing rate fluctuated without discernible trend during the 3-month period following the end of the eruption. The flux varied between 2 and 6 kg/s in the first weeks of March, then decreased and varied between 1 and 3 kg/s through the end of March. It became higher ($\sim 6 \text{ kg/s}$) and stable in April, then highly fluctuating again ($1\text{--}9 \text{ kg/s}$) by the end of May 2015. The lack of DOAS scans with the required characteristics (trough-shaped distribution with wind direction blowing towards the instrument) in the first weeks of May and the scarcity of scans in April may reflect the less favourable weather conditions for useful DOAS measurements during the transition between winter and spring seasons.

DOAS data from the Holuhraun eruption were processed until the end of May 2015 (Fig. 7), after which SO_2 from the lava flow field was below the detection limit of the instrument ($5 \text{ ppm}\cdot\text{m}$ for single spectra). Thus, the lava flow field formed during a 6-month-long eruption continued to release measurable SO_2 for 3 months after the eruption ended.

Contribution of Holuhraun lava flow field SO_2 emissions

Assuming that the average post-eruption flux of 3 kg/s was emitted constantly throughout the 3 months of this study, an estimated total of 24 kt of SO_2 was released during this period. This is equivalent to an additional 0.2% to the total of $\sim 11 \text{ Mt}$ of SO_2 that was released during the eruption. This estimated 24 kt of SO_2 , released during 3 months, is greater than the 16 kt of SO_2 emitted by Icelandic industry in 2013 (Centre on Emission Inventories and Projections, 2015). The SO_2 emitted by the lava flow field remained near ground level, resulting in high ground-level concentrations of SO_2 near to the eruption site and posing potential health hazards (including respiratory problems and eye irritation; Longo et al. 2008; Ilyinskaya et al. 2017) to people exposed to it. Access was therefore restricted to the area around the lava flow field until 1 June 2015, after a field visit by IMO on 19 May 2015 measured only minor emissions of SO_2 from fractures in the lava and from the main eruption crater (IMO, 2015c).

The Holuhraun eruption magma was highly rich in sulphur (Gauthier et al. 2016; Gíslason et al. 2015), resulting in high emissions of SO_2 at the vent. It is likely that the magma had a permeable bubble network during ascent allowing volatiles to be released from the magma to form the gas-rich eruption plume (e.g. Burton et al. 2007; Polacci et al. 2008). Therefore, when the lava was erupted, much of its sulphur content had already been released by efficient degassing at the vent, and so only a small proportion of SO_2 remained within the lava to be released during and after emplacement. Due to the large size of this flood basalt eruption, this small

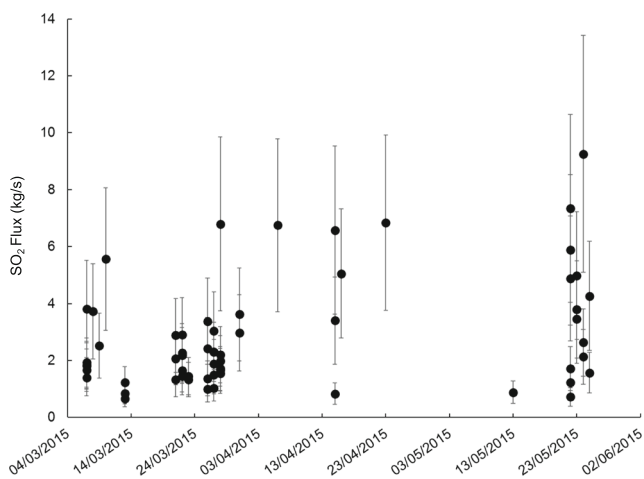


Fig. 7 Post-eruption SO_2 flux from the 2014–2015 Holuhraun lava flow field as recorded by ScanDOAS instrument MAYP111126. Labelled dates are at 10-day intervals, error bars are 45%

proportion of SO_2 released by the lava flow field was still a large and significant mass of SO_2 .

The petrologic approach of Thordarson et al. (1996) was used to calculate the portion of erupted lava responsible for outgassing the post-eruptive SO_2 . Degassed tephra glass contained 377 ppmw sulphur (Bali et al. 2017 Melt inclusion constraints on volatile systematics and degassing history of the 2014–2015 Holuhraun eruption, Iceland, submitted), and degassed lava contained 97 ppmw sulphur (Gauthier et al. 2016). The 24 kt of post-eruptive SO_2 are calculated to have been emitted from 4.23×10^{10} kg of the 3.56×10^{12} kg of lava produced by the Holuhraun eruption.

Lava flow field radiant heat flux

The radiant heat flux due to the Holuhraun lava flow field decreased following the end of the eruption (Fig. 8), from 13.3×10^3 MW on 8 February 2015 (in the final month of the eruption) to 6.9×10^3 MW on 10 March (10 days after the eruption ended), followed by a continued cooling. Once the eruption had ended, the source of hot lava was removed, and so all heat released was due to the cooling of the existing lava. The measured post-eruption SO_2 fluxes were emitted as this emplaced lava cooled.

Discussion

Cooling and outgassing of lava flows

Several studies have analysed the cooling and crystallisation of lava bodies (e.g. Keszthelyi and Denlinger, 1996; Wooster et al. 1997; Cashman et al. 1999; Patrick et al. 2004; Kolzenburg et al. 2016). Lava flows cool by thermal radiation and atmospheric convection from the surface and by

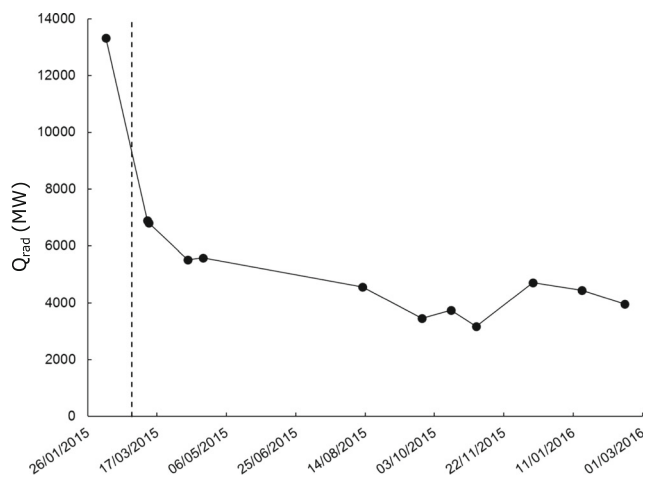


Fig. 8 Radiant heat flux calculated during the post-eruptive cooling phase of the Holuhraun lava flow field following Eq. 4. The vertical dashed line indicates the end of the eruption on 27 February 2015. Labelled dates are at 50-day intervals

conduction to the underlying country-rock (Keszthelyi and Denlinger, 1996; Neri, 1998; Patrick et al. 2004). Lava from the Holuhraun eruption had up to 45% vesicles (Lavallée et al. 2015). This high vesicularity is likely to have enhanced the cooling of the flows as lava porosity is considered to affect the rate of cooling, with more vesicular lava cooling more rapidly (Keszthelyi and Denlinger, 1996).

Processes that occur during cooling could contribute to the release of SO_2 from the lava flow. As an emplaced lava flow cools and solidifies post-eruption, it thermally contracts (Spry, 1962; Wittmann et al. 2017). Thermal contraction of lava results in the formation of cooling fractures such as brittle cracks and columnar jointing (Ryan and Sammis, 1978; Long and Wood, 1986; Reiter et al. 1987; Grossenbacher and McDuffie, 1995). Continued cooling causes fractures to propagate from the surface into the interior of the flow (Reiter et al. 1987; Aydin and DeGraff, 1988; Kattenhorn and Schaefer, 2008). Not only will fractures and cracks enhance the cooling of the lava flow interior, they will also provide pathways for volatiles to be released from the interior of the flow to the atmosphere (Fuller, 1938; Wilmoth and Walker, 1993).

Vesicles within a lava flow consist of both a primary population that were exsolved from the melt during eruption and a secondary population that were exsolved during cooling and crystallisation (Cashman et al. 1994). The strength of the cooling lava crust will prevent the upward migration of bubbles, causing volatiles to remain trapped within the flow (Polacci and Papale, 1997). Volatiles exsolved from the lava therefore contribute to the formation of a low permeability vesicle network in which the volatiles become trapped, with inefficient outgassing due to the formation of a solid outer crust on the lava flow. The outgassing efficiency will be dependent on the permeability of the lava flow (Burgisser and



Fig. 9 A photo taken during a surveillance flight on 4 November 2014 showing gases being released from cooling fractures in the lava flow field (highlighted by arrows). Gases include H₂O (both magmatic and meteoric), SO₂, and CO₂. Photo by M. Hensch, IMO

DeGruyter, 2015; Kennedy et al. 2016), with the permeability dependent on vesiculation history (Saar and Manga, 1999; Wright et al. 2009). Fracturing of the lava will then create high permeability pathways allowing efficient outgassing of these trapped volatiles, as seen at the Holuhraun lava flow field (Fig. 9).

Extraction of gas from the lava flow should be most efficient where it is highly fractured, which will be where the thermal contraction is greatest. The formation of high permeability pathways through propagation of cooling fractures would account for the fact that SO₂ was released from the Holuhraun lava flow field for several months after lava flow emplacement and that over this time, the SO₂ flux did not decrease concurrently with the decrease in thermal emission. SO₂ flux is not a simple decay correlated with lava cooling, as both volatile availability and fracture propagation produce the SO₂ flux. As fractures provide a pathway for gas to escape, outgassing is able to continue as fracture propagation continues to tap volatiles trapped in the cooling flow interior. The episodic nature of fracture propagation (Ryan and Sammis, 1978; DeGraff and Aydin, 1987; Reiter et al. 1987) would explain the fluctuating post-eruption SO₂ flux.

Using a petrological method, Thordarson et al. (1996) calculated that of the SO₂ released by the 1783–1784 Laki eruption, 20% was released by lava flows during their emplacement and cooling. This is two orders of magnitude larger than our calculated value of 0.2% of SO₂ released by the Holuhraun lava flow field in the 3 months following the eruption. The reason for this large discrepancy is that our measurements only began after the eruption had ended. The Holuhraun eruption lasted for 6 months, and therefore, lava flows had been outgassing for up to 6 months before our study even began, and so a significant proportion of the outgassing has not been captured. Outgassing from lava flows is likely to have been greatest during emplacement, when mechanical breakup of the lava crust facilitated gas release (Polacci and

Papale, 1997; Soule and Cashman, 2004), and we did not capture syn-emplacment outgassing during our study.

Conclusions

Scanning DOAS instruments were installed at the eruption site of the 2014–2015 Holuhraun eruption to monitor the flux of SO₂. Based on a novel approach to measure emissions from the emplaced lava flow field, we found that this lava flow field continued to release SO₂ for 3 months after the end of the eruption. During this time, SO₂ flux from the lava flow field varied from < 1 to 9 kg/s, and a post-eruption average flux of 3 kg/s was calculated. The post-eruption Holuhraun lava flow field was a significant source of environmental pollution, releasing 24 kt of SO₂ in the 3 months after the eruption. This post-eruption lava flow field SO₂ flux contributed an additional 0.2% to the ~11 Mt total eruption SO₂ emissions in the 3 months following the eruption. This emission remained near ground level, posing health hazards, which resulted in access to the area being restricted until 1 June 2015, 3 months after the eruption ended. During solidification, SO₂ can be outgassed, we propose, by fracture propagation as high permeability pathways are developed, allowing gas to be released for several months after the end of the eruption. We show that this release is not a simple decay correlated with lava cooling, as both volatile availability and fracture propagation produce a fluctuating SO₂ flux.

Acknowledgements The installation of the DOAS instruments at Holuhraun were funded by FUTUREVOLC and a Swedish FORMAS grant (2014-1848). We gratefully thank Baldur Bergsson and staff at the Icelandic Meteorological Office for installing and maintaining the equipment. Photos by Baldur Bergsson (Figure 1) and Martin Hensch (Figures 3 and 9) are used with kind permission from the Icelandic Meteorological Office. The NovacProgram software was developed by M. Johansson and Y. Zhang. The authors thank Christoph Kern, Andrew Harris, and an anonymous reviewer for their comments and suggestions which have greatly improved this manuscript.

Open Access This article is distributed under the terms of the Creative Commons Attribution 4.0 International License (<http://creativecommons.org/licenses/by/4.0/>), which permits unrestricted use, distribution, and reproduction in any medium, provided you give appropriate credit to the original author(s) and the source, provide a link to the Creative Commons license, and indicate if changes were made.

References

- Aydin A, DeGraff JM (1988) Evolution of polygonal fracture patterns in lava flows. *Science* 239:471–476
- Barsotti S, Jóhannsson T, Hellsing VÚ, Pfeffer MA, Guðnason T, Stefánsdóttir G (2015) Abundant SO₂ release from the 2014 Holuhraun eruption (Bárðarbunga, Iceland) and its impact on human health. *Geophys Res Abstr* 17:EGU2015–EG12886

- Bluth GJS, Shannon JM, Watson IM, Prata AJ, Realmuto VJ (2007) Development of an ultra-violet digital camera for volcanic SO₂ imaging. *J Volcanol Geotherm Res* 161:47–56
- Bobrowski N, Kern C, Platt U, Hörmann C, Wagner T (2010) Novel SO₂ spectral evaluation scheme using the 360–390 nm wavelength range. *Atmos Meas Tech* 3:879–891
- Bottinga Y, Javoy M (1991) The degassing of Hawaiian tholeiite. *Bull Volcanol* 53:73–85
- Burgisser, A., Degruyter, W., 2015. Magma ascent and degassing at shallow levels Sigurdsson, H., Houghton, B., McNutt, S. R., Rymer, H., Stix, J., (Eds), In: *The Encyclopedia of Volcanoes*, second edition
- Burton MR, Mader HM, Polacci M (2007) The role of gas percolation in quiescent degassing of persistently active basaltic volcanoes. *Earth Plan Sci Let* 264:46–60
- Cashman KV, Mangan MT, Newman S (1994) Surface degassing and modification to vesicle size distributions in active basalt flows. *J Volcanol Geotherm Res* 61:45–68
- Cashman KV, Thornber C, Kauahikaua JP (1999) Cooling and crystallisation of lava in open channels, and the transition of Pāhoehoe Lava to ‘A’ā. *Bull Volcanol* 61:306–323
- Centre on Emission Inventories and Projections, European Monitoring and Evaluation Programme, 2015. http://www.ceip.at/ms/ceip_home1/ceip_home/data_viewers/official_tableau/. Accessed 3 June 2016
- Coppola D, Laiolo M, Cigolini C, Delle Donne D, Ripepe M (2016) Enhanced volcanic hot-spot detection using MODIS IR data: results from the MIROVA system. *Geol Soc Lond Spec Publ* 426:181–205. <https://doi.org/10.1144/SP426.5> In: Harris, A. J. L., De Groeve, T., Garel, F., Cam, S. A., (Eds.), *Detecting, modelling and responding to effusive eruptions*
- Coppola D, Ripepe M, Laiolo M, Cigolini C (2017) Modelling satellite-derived magma discharge to explain caldera collapse. *Geology* 45(6):523–526. <https://doi.org/10.1130/G38866.1>
- DeGraff JM, Aydin A (1987) Surface morphology of columnar joints and its significance to mechanics and direction of joint growth. *Geol Soc Am* 99:605–617
- Edmonds M, Herd RA, Galle B, Oppenheimer C (2003) Automated, high time-resolution measurements of SO₂ flux at Soufrière Hills Volcano, Montserrat. *Bull Volcanol* 65:578–586
- Edner H, Ragnarson P, Svanberg S, Wallinder E, Ferrara R, Cioni R, Raco B, Taddeucci G (1994) Total fluxes of sulfur dioxide from the Italian volcanoes Etna, Stromboli and Vulcano measured by differential absorption lidar and passive differential optical absorption spectroscopy. *J Geophys Res* 99:827–838
- Fuller RE (1938) Deuteric alteration controlled by the jointing of lavas. *Am J Sci* 25:161–171
- Galle B, Oppenheimer C, Geyer A, McGonigle AJS, Edmonds M, Horrocks L (2002) A miniaturised ultraviolet spectrometer for remote sensing of SO₂ fluxes: a new tool for volcano surveillance. *J Volcanol Geotherm Res* 119:241–254
- Galle, B, Johansson, M, Rivera, C, Zhang, Y, Kihlman, M, Kern, C, Lehmann, T, Platt, U, Arellano, S, Hidalgo, S, (2010). Network for Observation of Volcanic and Atmospheric Change (NOVAC)—a global network for volcanic gas monitoring: network layout and instrument description. *J Geophys Res* 115. <https://doi.org/10.1029/2009JD011823>
- Gauthier PJ, Sigmarsson O, Gouhier M, Haddada B, Moune S (2016) Elevated gas flux and trace metal degassing from the 2014–2015 fissure eruption at the Bárðarbunga volcanic system, Iceland. *J Geophys Res Solid Earth* 121:1610–1630. <https://doi.org/10.1002/2015JB012111>
- Gislason SR, Stefánsdóttir G, Pfeffer MA, Barsotti S, Jóhannsson T, Galeczka I, Bali E, Sigmarsson O, Stefánsson A, Keller NS, Sigurdsson Á, Bergsson B, Galle B, Jacobo VC, Arellano S, Aiuppa A, Jónasdóttir EB, Eiríksdóttir ES, Jakobsson S, Guðfinnsson GH, Halldórson SA, Gunnarsson H, Haddadi B, Jónsdóttir I, Thordarson T, Riihuus M, Högnadóttir T, Dürig T, Pedersen GBM, Höskuldsson Á, Gudmundsson MT (2015) Environmental pressure from the 2014–15 eruption of Bárðarbunga volcano, Iceland. *Geochemical Perspective Letters* 1: 84–93
- Grainger JF, Ring J (1962) Anomalous Fraunhofer line profiles. *Nature* 193:762
- Grossenbacher KA, McDuffie SM (1995) Conductive cooling of lava: columnar joint diameter and stria width as functions of cooling rate and thermal gradient. *J Volcanol Geotherm Res* 69:95–103
- Hirabayashi J, Ohba T, Nogami K (1995) Discharge rate of SO₂ from Unzen volcano, Kyushu, Japan. *Geophys Res Let* 22:1709–1712
- Icelandic Meteorological Office, 2014. Bárðarbunga 2014 – November events, <http://en.vedur.is/earthquakes-and-volcanism/articles/nr/3023>. Accessed 28 September 2015
- Icelandic Meteorological Office, 2015a. Bárðarbunga 2015 – February events, <http://en.vedur.is/earthquakes-and-volcanism/articles/nr/3087>. Accessed 28 September 2015
- Icelandic Meteorological Office, 2015b. Bárðarbunga 2015 – January events, <http://en.vedur.is/earthquakes-and-volcanism/articles/nr/3071>. Accessed 28 September 2015
- Icelandic Meteorological Office, 2015c. Bárðarbunga 2015 – March, April, May <http://en.vedur.is/earthquakes-and-volcanism/articles/nr/3122>. Accessed 3 July 2017
- Ilyinskaya E, Schmidt A, Mather TA, Pope FD, Witham C, Baxter P, Jóhannsson T, Pfeffer M, Barsotti S, Singh A, Sanderson P (2017) Understanding the environmental impacts of large fissure eruptions: aerosol and gas emissions from the 2014–2015 Holuhraun eruption (Iceland). *Earth Planet Sci Lett* 472:309–322
- Jousset P, Budi-Santoso A, Jolly AD, Boichi M, Suroño D, Sumarti S, Hidayati S, Thierry P (2013) Signs of magma ascent in LP and VLP seismic events and link to degassing: an example from the 2010 explosive eruption at Merapi volcano, Indonesia. *J Volcanol Geotherm Res* 261:171–192
- Kattenhorn SA, Schaefer CJ (2008) Thermal-mechanical modelling of cooling history and fracture development in inflationary basalt lava flows. *J Volcanol Geotherm Res* 170:181–197
- Kennedy BM, Wadsworth FB, Vasseur J, Schipper CI, Jellinek AM, von Aulock FW, Hess K, Russell JK, Lavallée Y, Nichols ARL, Dingwell DB (2016) Surface tension driven processes densify and retain permeability in magma and lava. *Earth Plan Sci Let* 433:116–124
- Keszthelyi L, Denlinger R (1996) The initial cooling of pāhoehoe flow lobes. *Bull Volcanol* 58:5–18
- Kolzenburg S, Giordano D, Cimarelli C, Dingwell DB (2016) In situ thermal characterisation of cooling/crystallising lavas during rheology measurements and implications for lava flow emplacement. *Geochimica et Cosmochimica Acta* 195:244–258
- Kyle PR, Sybeldon LM, McIntosh WC, Meeker K, Symonds R (1994) Sulphur dioxide emission rates from Mount Erebus, Antarctica. *Am Geophys Union*:69–82 In: Kyle, P. R., (Ed) *Volcanological and environmental studies of Mount Erebus, Antarctica* 66
- Lavallée Y, Kendrick J, Wall R, von Aulock F, Kennedy B, Sigurdsson F (2015) Experimental constraints on the rheology and mechanical properties of lava erupted in the Holuhraun area during the 2014 rifting event at Bárðarbunga, Iceland. *Geophys Res Abstr* 17: EGU2015–EG11544
- Long PE, Wood BJ (1986) Structures, textures and cooling histories of Columbia River basalt flows. *Geol Soc Am Bull* 97:1144–1155
- Longo BM, Rossignol A, Green JB (2008) Cardiorespiratory health effects associated with sulphurous volcanic air pollution. *Public Health* 122:809–820
- Malinconico LL (1979) Fluctuations in SO₂ emission during recent eruptions of Etna. *Nature* 278:43–45
- McGonigle AJS, Oppenheimer C, Galle B, Mather T, Pyle D., 2002. Walking traverse and scanning DOAS measurements of volcanic

- gas emission rates. *Geophys Res Lett.* <https://doi.org/10.1029/2002GL015827>
- Moffat AJ, Millan MM (1971) The applications of optical correlation techniques to the remote sensing of SO₂ plumes using sky light. *Atmos Environ* 5:677–690
- Mori T, Burton M (2006) The SO₂ camera: a simple, fast and cheap method for ground-based imaging of SO₂ in volcanic plumes. *Geophys Res Lett* 33:L24804. <https://doi.org/10.1029/2006GL027916>
- Mori T, Mori T, Kazahaya K, Ohwada M, Hirabayashi J, Yoshikawa S (2006) Effect of UV scattering on SO₂ emission rate measurements. *Geophys Res Lett* 33:L17315. <https://doi.org/10.1029/2006GL026285>
- Neri A (1998) A local heat transfer analysis of lava cooling in the atmosphere: application to thermal diffusion-dominated lava flows. *J Volcanol Geotherm Res* 81:215–243
- Palma JL, Calder ES, Basualto D, Blake S, Rothery DA (2008) Correlations between SO₂ flux, seismicity and outgassing activity at the open vent of Villarrica volcano, Chile. *J Geophys Res* 113: B10201. <https://doi.org/10.1029/2008JB005577>
- Palma JL, Blake S, Calder ES (2011) Constraints on the rates of degassing and convection in basaltic open-vent volcanoes. *Geochem Geophys Geosyst* 12:Q11006. <https://doi.org/10.1029/2011GC003715>
- Patrick MR, Dehn J, Dean K (2004) Numerical modelling of lava flow cooling applied to the 1997 Okmok eruption: approach and analysis. *J Geophys Res* 109:B03202. <https://doi.org/10.1029/2003JB002537>
- Pedersen GBM, Höskuldsson Á, Dürig T, Thordarson T, Jónsdóttir I, Riihuus MS, Óskarsson BV, Dumont S, Magnusson E, Gudmundsson MT, Sigmundsson F, Drouin VJPB, Gallagher C, Askew R, Gudnason J, Moreland WM, Nikkola P, Reynolds HI, Schmith J, the IES eruption team (2017) Lava field evolution and emplacement dynamics of the 2014–2015 basaltic fissure eruption at Holuhraun, Iceland. *J Volcan Geotherm Res* 340:155–169
- Platt, U., Stutz, J., (2008). Differential absorption spectroscopy. In: Platt, U, Stutz, J, Differential Optical Absorption Spectroscopy, Physics of Earth and Space Environments, Springer 135–174. https://doi.org/10.1007/978-3-540-75776-4_6
- Platt U, Perner D, Pätz HW (1979) Simultaneous measurement of atmospheric CH₂O, O₃, and NO₂ by differential optical absorption. *J Geophys Res* 84:6329–6335
- Platt U, Lübcke P, Kuhn J, Bobrowski N, Prata F, Burton M, Kern C (2015) Quantitative imaging of volcanic plumes—results, needs, and future trends. *J Vol Geotherm Res* 300:7–21
- Polacci M, Papale P (1997) The evolution of lava flows from ephemeral vents at Mount Etna: Insights from vesicle distribution and morphological studies. *J Volcanol Geotherm Res* 76:1–17
- Polacci M, Baker DR, Bai L, Mancini L (2008) Large vesicles record pathways of degassing at basaltic volcanoes. *Bull Volcanol* 70: 1023–1029. <https://doi.org/10.1007/s00445-007-0184-8>
- Reiter M, Barroll MW, Minier J, Clarkson G (1987) Thermo-mechanical model for incremental fracturing in cooling lava flows. *Tectonophysics* 142:241–260
- Ryan MP, Sammis CG (1978) Cyclic fracture mechanisms in cooling basalt. *Geol Soc Am* 89:1295–1308
- Saar MO, Manga M (1999) Permeability-porosity relationship in vesicular basalts. *Geophys Res Lett* 26:111–114
- Sawyer GM, Carn SA, Tsanev VI, Oppenheimer C, Burton M (2008) Investigation into magma degassing at Nyiragongo volcano, Democratic Republic of the Congo. *Geochem Geophys Geosyst* 9: Q02017. <https://doi.org/10.1029/2007GC001829>
- Schmidt A, Leadbetter S, Theys N, Carboni E, Witham CS, Stevenson JA, Birch CE, Thordarson T, Turnock S, Barsotti S, Delaney L, Feng W, Grainger RG, Hort MC, Höskuldsson Á, Ialongo I, Ilnskaya E, Jóhannsson T, Kenny P, Mather TA, Richards NAD, Shepherd J, (2015) Satellite detection, long-range transport and air quality impacts of volcanic sulphur dioxide from the 2014–2015 flood lava eruption at Bárðarbunga (Iceland). *J Geophys Res-Atmos* 120. <https://doi.org/10.1002/2015JD023638>
- Soule SA, Cashman KV (2004) The mechanical properties of solidified polyethylene glycol 600, an analogue for lava crust. *J Volcanol Geotherm Res* 129:139–153
- Sparks RSJ (2003). Dynamics of magma degassing. In: Oppenheimer D, Pyle D, Barclay J, (Eds) *Volcanic Degassing*, Geol Soc Spec Publ 213:5–22
- Sparks RSJ, Pinkerton H (1978) Effect of degassing on rheology of basaltic lava. *Nature* 276:385–386
- Spry A (1962) The origin of columnar jointing, particularly in basalt flows. *J Geol Soc Australia* 8:191–216. <https://doi.org/10.1080/14400956208527873>
- Stoiber RE, Malinconico LL, Williams SN (1983) Use of the correlation spectrometer at volcanoes. In: Tazieff H, Sabroux J (eds) *Forecasting Volcanic Events*. Elsevier, pp 425–444
- Stutz J, Platt U (1996) Numerical analysis and estimation of the statistical error of differential optical absorption spectroscopy measurements with least-squares methods. *Appl Opt* 35:6041–6053
- Swanson DA, Fabbi BP (1973) Loss of volatiles during fountaining and flowage of basaltic lava at Kilauea volcano, Hawaii. *J Res US Geol Surv* 1:649–658
- Thordarson T, Larsen G (2007) Volcanism in Iceland in historical time: volcano types, eruption styles and eruptive history. *J Geodyn* 43:118–152
- Thordarson T, Self S (2003) Atmospheric and environmental effects of the 1783–1784 Laki eruption: a review and reassessment. *J Geophys Res* 108:D1. <https://doi.org/10.1029/2001JD002042>
- Thordarson T, Self S, Óskarsson N (1996) Sulphur, chlorine and fluorine degassing and atmospheric loading by the 1783–1784 AD Laki (Skaftár Fires) eruption in Iceland. *Bull Volcanol* 58:205–225
- Thordarson, T., Self, S., Miller, D. J., Larsen, G., Vilmundardóttir, E. G., 2003. Sulphur release from flood lava eruptions in the Veidivötn, Grímsvötn and Katla volcanic systems, Iceland. In: Oppenheimer, C., Pyle, D. M., Barclay, J., (Eds.) *Volcanic Degassing*. The Geological Society of London, Special Publications 213:103–121
- Umhverfisstofnun (2016) Loftgæðamælingar á Íslandi <http://www.ust.is/default.aspx?pageid=14da32aa-8362-4378-a165-d3a2a6d6f1c6&station=reyardarfjordur1hjallaleira>. Accessed 17 June 2016
- Walker GPL (1989) Spongy pāhoehoe in Hawaii: a study of vesicle-distribution patterns in basalt and their significance. *Bull Volcanol* 51:199–209
- Weibring P, Edner H, Svanberg S, Cecchi G, Pantani L, Ferrara R, Caltabiano T (1998) Monitoring of volcanic sulphur dioxide emissions using differential absorption lidar (DIAL), differential optical absorption spectroscopy (DOAS), and correlation spectroscopy (COSPEC). *Appl Phys* 67:419–426
- Wilmoth RA, Walker GPL (1993) P-type and S-type pāhoehoe: a study of vesicle distribution patterns in Hawaiian lava flows. *J Volcanol Geotherm Res* 55:129–142
- Wittmann W, Sigmundsson F, Dumont S, Lavallée Y (2017) Post-emplacement cooling and contraction of lava flows: InSAR observations and a thermal model for lava fields at Hekla volcano, Iceland. *J Geophys Res Solid Earth* 122:946–965. <https://doi.org/10.1002/2016JB013444>
- Wooster MJ, Wright R, Blake S, Rothery DA (1997) Cooling mechanisms and an approximate thermal budget for the 1991–1993 Mount Etna lava flow. *Geophys Res Lett* 24:3277–3280
- Wooster MJ, Zhukov B, Oertel D (2003) Fire radiative energy for quantitative study of biomass burning: derivation from the BIRD experimental satellite and comparison to MODIS fire products. *Remote Sens Environ* 86:83–107
- Wright HMN, Cashman KV, Gottesfeld EH, Roberts JJ (2009) Pore structure of volcanic clasts: measurements of permeability and electrical conductivity. *Earth Planet Sc Lett* 280: 93–104